




Article

Developing Bio-Nano Composites Using Cellulose-Nanofiber-Reinforced Epoxy

Meysam Mehdinia ¹, Mohammad Farajollah Pour ², Hossein Yousefi ³, Ali Dorieh ^{4,*}, Anthony J. Lamanna ⁵  and Elham Fini ^{5,*}

¹ Wood and Forest Products Science Research Division, Research Institute of Forests and Rangelands, Agricultural Research Education and Extension Organization (AREEO), Tehran 13185-116, Iran; meysammehdinia@gmail.com

² Department of Wood and Science & Technology, Faculty of Natural Resource, University of Tehran, Karaj 31587-77871, Iran; moh.farajollahpour@gmail.com

³ Department of Wood Engineering and Technology, Gorgan University of Agricultural Sciences and Natural Resources, Gorgan 49138-15739, Iran; hyousefi@gau.ac.ir

⁴ Department of Wood Processing and Biomaterials, Faculty of Forestry and Wood Sciences, Czech University of Life Sciences Prague, Prague 99991-2570, Czech Republic

⁵ School of Sustainable Engineering and the Built Environment, Ira A. Fulton Schools of Engineering, Arizona State University, 660 S. College Avenue, Tempe, AZ 85287-3005, USA; drtony@asu.edu

* Correspondence: ali.dorieh@yahoo.com (A.D.); efini@asu.edu (E.F.)

Abstract: This study introduces the development of a novel bio-nano composite via the dispersion of cellulose nanofibers (CNF) in epoxy. The surface of cellulose nanofibers was functionalized using a two-step chemical treatment to enhance dispersion. The interfacial characteristics of CNF were improved using alcohol/acetone treatments. The modified CNF (M-CNF) demonstrated enhanced compatibility and improved dispersion in the epoxy matrix as evidenced by scanning electron microscopy. Based on the analysis of X-ray diffraction patterns, M-CNF did not disturb the crystalline phases at the interface. The results of mechanical testing showed that M-CNF worked as a reinforcing agent in the bio-nano composite. The flexural modulus increased from 1.4 to 3.7 GPa when M-CNF was introduced. A similar trend was observed for tensile strength and impact resistance. The optimum performance characteristics were observed at M-CNF of 0.6%. At higher dosages, some agglomeration was observed, which weakened the interfacial properties. This study promotes sustainability and resource conservation while offering CNF as a sustainable reinforcing agent to develop bio-nano composites.

Keywords: composite; cellulose nanofiber; epoxy; bio-nano composite; modulus



Citation: Mehdinia, M.; Farajollah Pour, M.; Yousefi, H.; Dorieh, A.; Lamanna, A.J.; Fini, E. Developing Bio-Nano Composites Using Cellulose-Nanofiber-Reinforced Epoxy. *J. Compos. Sci.* **2024**, *8*, 250. <https://doi.org/10.3390/jcs8070250>

Academic Editors: Ahmed Koubaa, Mohamed Ragoubi and Frédéric Becquart

Received: 22 April 2024

Revised: 18 June 2024

Accepted: 27 June 2024

Published: 1 July 2024



Copyright: © 2024 by the authors. Licensee MDPI, Basel, Switzerland. This article is an open access article distributed under the terms and conditions of the Creative Commons Attribution (CC BY) license (<https://creativecommons.org/licenses/by/4.0/>).

1. Introduction

In modern society, polymer-based materials are extensively used in the manufacturing of friction engineering components such as gears, bearings, cams, parts covered with polymer films, etc. [1–3].

Two categories of polymer-based materials can be distinguished based on the thermal behavior. Polymeric materials that undergo melting or softening upon exposure to heat and solidify when cooled are called thermoplastic resins. They can be melted, reformed and reprocessed, and develop new structure through heating and cooling cycles without inducing any chemical change or degradation. In contrast, thermoset resins (or thermosetting) are usually cured or hardened with the application of heat, and once they are formed, these cannot be remolten or reformed [4].

Epoxy resins, multipurpose thermosetting polymers, have attracted wide industrial interest. Epoxy resin contains epoxide reactive groups in its structure that can crosslink with various functional groups such as amine, carboxyl, and hydroxyl [5].

The carbon–oxygen–carbon of linkage in epoxy resin can form a reaction with hydroxyl, carboxyl, and amine groups of other polymers, which act as a bridge to connect other polymers. This linkage improves crosslinking inside a polymer and interfacial adhesion between two polymers mixed, which improves overall properties [6]. Their performance is characterized by their superior adhesive properties, fast reactivity, dimensional stability, capability as electrical insulation, and resistance to chemical corrosion [7,8].

There have been several studies on developing nanoscale fillers including carbon nanoparticles, nano clay, TiO_2 , SiO_2 , CaCO_3 , and Al_2O_3 for use in polymeric matrices to improve their performance [9,10]. These nanofillers were introduced to various polymeric matrices such as thermosets, thermoplastics, elastomers either in isolation or in combination. Dramatic enhancements in thermal stability, mechanical, chemical, and physical properties were observed in nanoparticle-loaded polymer composites [11–15]. There has been an emphasis on biodegradable sources of these reinforcing agents over the years to enhance the sustainability and reduce the carbon footprint of these composites [16]. Plant fibers have drawn significant attention to improve the durability of composites owing to their stratified structure [17–19].

One of the best areas to use fibers is polymer reinforcing. Attempts to reinforce thermosetting composites with various types of additives with a wide range of dimensions have been successful [20–26]. Renewable, biodegradable sources of these reinforcing agents would be promising. Plant fibers have drawn consideration because of their unique stratified structure, which has been broadly engaged to improve the durability of the composites.

Moudood et al. explored the durability and mechanical performance (tensile and flexural behavior) of flax/bio-epoxy composites exposed to different environmental conditions. Flax/bio-epoxy composites were exposed to different environmental conditions: water immersion, high humidity and freeze/thaw cycling. The tensile strength and modulus are decreased approximately by 9% and 57%, respectively, for water-saturated samples compared to as manufactured samples. The results showed that flax/bio epoxy composites can be used in most environmental conditions, excluding underwater applications which cause degradation of the properties [27].

The effect of adding different contents of 3-methoxy silyl propyl amine-modified nanozirconia particles on flexural and tensile strength of basalt fibers/epoxy composites was investigated by Azizi et al. According to the results obtained from the three-point flexural and tensile tests, flexural strength, flexural modulus, flexural failure strain, tensile strength, tensile modulus and tensile failure strain enhanced by 90, 74, 84, 76, 85 and 14%, respectively, by adding 3 wt.% nanozirconia [28].

Among various natural fibers, cellulose has by far been demonstrated to be the most promising candidate with regard to its availability from various resources, as it can be found in plants, algae, tunicates, and some bacteria [29,30]. Cellulose fibers, especially at nano size, demonstrate exclusive characteristics such as extreme aspect ratio, high stiffness and strength, and lightweight [31–33].

While a forward-looking and fascinating polymer that has been seen as an inexhaustible source of raw materials which has a high potential for modification and functionalization with several available industrial uses, there is still plenty to discover in cellulose [34–36]. The characteristics of cellulose, particularly mechanical properties, can be further extended when cellulose chains in highly ordered regions are bundled together into nano-particles or nanocelluloses [37].

Cellulose is the most abundant biological material on Earth, with an annual production of more than 1.5 trillion tons [38,39]. Nanocellulose refers to nanostructured cellulose that can be produced from cellulose-derived materials [40]. Nanocellulose is mainly classified into cellulose nanocrystal (CNC), cellulose nanofiber (CNF), and bacterial nanocellulose (BNC) [41]. Among them, CNFs have become of great interest to many researchers to improve the mechanical characteristics of fiber-reinforced composites due to their high specific strength, stiffness, aspect ratio, excellent mechanical properties, and environmen-

tally friendly nature [42–45]. CNFs are considered to be the best substance to create a novel bio-composite industry [46].

The interaction between the plant fibers and the polymer matrix is essential for high-quality results. Mechanical interlocking is prevented by the smooth surface of CNF. Regarding chemical compatibility, CNFs are hydrophilic and the epoxy matrix is hydrophobic, making interfacial interactions notably weak. Epoxy composites do not perform well in these opposing conditions. Thus, treatments are needed to improve the interfacial bonding between CNF and epoxy composites. Generally, these modification treatments can be grouped into two categories: chemical processes, and physical processes [47,48].

Indeed, cellulose has three hydroxyl groups per repeating unit, which makes it readily susceptible to chemical modifications [49]. Among the studied chemical processes, mercerization [50], silanization [51], oxidation [52], esterification [53], grafting of branched/hyperbranched polymers stand out [54].

The type of modification process must be carefully selected because of the desired features of the composite, the uniformity and balance of the process performance, the potential impacts on the CNF's structure and aspect ratio, the complexity of the formulation, environmental issues, and the capability for efficient scale-up of the process. The CNF aspect ratio is a key parameter governing the overall performances of the CNF/polymer composites which depend on the CNF's source and pretreatment. However, there are also other highly important process parameters. For example, the dispersion of fibrillated nanocellulose, which depends on mixing, has been recently identified as a key parameter for other similar applications [55,56]. In general, their behavior and effect on the composite matrix are mainly related to the colloidal properties that determine their self-assembly and stability mechanisms, as well as their interaction with the particles present in the matrix [57–59]. Therefore, the aspect ratio, dispersion, and 3D network stability, among other colloidal properties, will change some properties, such as its rheology [60,61].

In addition, CNF surfaces are rich in hydroxyl groups, which have a strong affinity for water. Under moist conditions, CNFs absorb a significant amount of water, primarily in the less ordered regions within the fibrils (reducing intrinsic CNF properties) and on the surface. Moreover, its inherent hydrophilicity makes CNF incompatible with hydrophobic polymers used as matrices in composites.

Several surface modification methods have been proposed to address the challenges described. They are generally based on covalent methods such as acetylation [62], esterification [63], silylation [64], grafting [65,66], or electrostatic methods based on counterions [67,68]. The general strategy is to hydrophobize the CNF surface to increase the hydromechanical stability and/or impart better compatibility with hydrophobic polymers. Covalent reactions are generally carried out in an organic solvent medium, where excess chemicals are required and the recovery of grafted nanoparticles is tedious and complex. The cost for this type of modification would likely be high.

In this study, we examined an easily implemented, efficient procedure to incorporate CNF into epoxy with enhanced compatibility. The problem of incompatibility between CNF and epoxy was reduced by functionalizing the hydroxyl groups of CNFs to make modified CNF (M CNF). The modification method developed in this study allows for the direct addition of M-CNF to the epoxy composite. This study also investigated the effects of the chemical variation in M-CNF on the dispersion characteristics of M-CNF, as well as the performance of the epoxy nanocomposite.

2. Experimental Materials and Methods

2.1. Raw Materials

A low-viscosity unfilled epoxy system was supplied by Huntsman Corporation (Salt Lake City, UT, USA). RenLam[®] M-1 was the first component, had a viscosity of 1425 mPas, a pot life of 30 min, and a specific gravity of 1.1 g·cm⁻³ at 25 °C. Ren[®] HY 956, with a viscosity of 420 mPas and a specific gravity of 1 g·cm⁻³, was used as a second component.

The mixing ratio of the two components was 100:20 parts by weight for the RenLam[®] M-1 and the Ren[®] HY 956, respectively. The hardener was unmodified cyclic aliphatic amine.

A gel of cellulose nanofibers (2.5 wt %) was prepared by Nano Novin Polymer Co (Sari, Iran). CNFs were mechanically prepared from sugar cane bagasse with an average diameter of 32 nm, and density of 1.6 g·cm⁻³ (Figure 1). Acetone (99% purity) and ethanol (99.8% purity) were added as modifier agents, supplied by Merck Co. (Darmstadt, Germany), to increase nanofiber and epoxy compatibility.

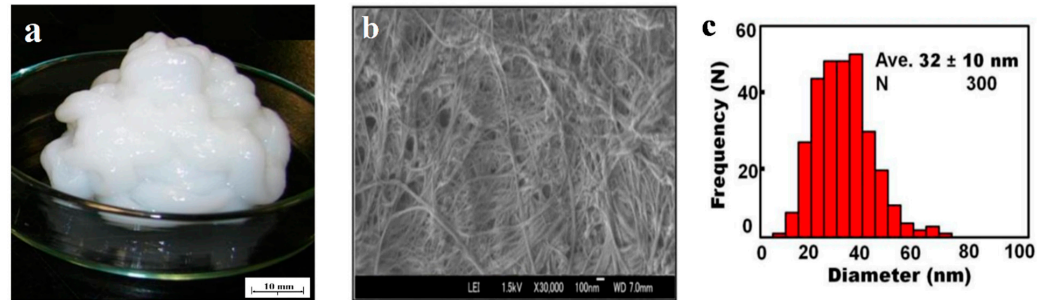


Figure 1. (a) Cellulose nanofiber gel, (b) morphology, and (c) size distribution of cellulose nanofibers.

2.2. Methods

2.2.1. Fabrication of Epoxy Nanocomposite with Modified CNF

CNF is hydrophilic, while epoxy is hydrophobic. The incompatible natures of CNF and epoxy resin make it almost impossible to produce a nanocomposite with untreated materials, where they shape separated and immiscible phases in the matrix even after ultrasonication (Figure 2f). Modifications were applied to exchange the interfacial functional groups to improve the miscibility of CNF in an epoxy matrix. The following steps were taken to prepare M-CNF.

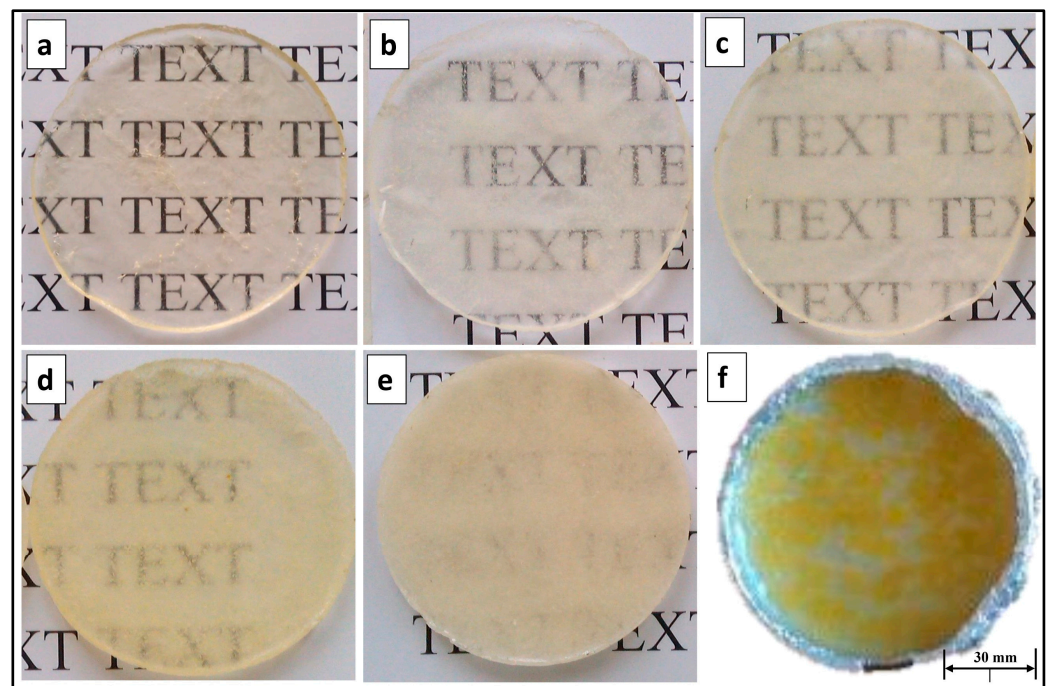


Figure 2. Photographs of samples of epoxy nanocomposite: (a) pure epoxy resin; (b–e) epoxy resin with M-CNF at doses of (b) 0.2%, (c) 0.4%, (d) 0.6%, and (e) 0.8%; (f) epoxy resin with 0.4% unmodified CNF.

1. To remove impurities and agglomerated fibers, 100 g of CNF gel was rinsed through a polyester sieve (40 μm).
2. The remaining CNF was dispersed in 250 mL of ethanol and stirred for 3 h with a magnetic stirrer.
3. Using a polyester mesh, the alcohol was separated from the nanofibers.
4. The treated nanofibers were dispersed and stirred in 250 mL of acetone. Similar to the first step, separation was carried out after 3 h of mixing to ensure that the modification process was complete.
5. Steps 1–4 were repeated three times.
6. To ensure the complete removal of water, ethanol, and acetone from the CNF, the CNF was centrifuged at a rotation speed of 12,000 rpm for 10 min.

The modified CNF (M-CNF) was stored in non-porous plastic bags at a temperature below 5 °C. In the next step, epoxy resin was heated to 50 \pm 5 °C. Epoxy nanocomposites were fabricated by separately adding 0.2%, 0.4%, 0.6%, and 0.8% based on the weight of the epoxy resin. The composite was subjected to ultrasonication by UHP-400 (Topsonics, Tehran, Iran), with two 3 min mixing intervals to promote homogenization. The curing agent was added and the composite was mixed for 30 s. Afterward, the nanocomposite was poured into a Petri dish and left to cure for 24 h at room temperature. A wax-release agent was used to facilitate the separation of the M-CNF/epoxy nanocomposite. The thickness of the produced nanocomposite films was set to 3 mm (Figure 2a–e). The characterizations of the epoxy nanocomposites are displayed in Table 1.

Table 1. Viscosity, density, and pH of samples of epoxy resins with varied contents of M-CNF.

| M-CNF Content (%) | 0 | 0.2 | 0.4 | 0.6 | 0.8 |
|---|---------------------------|---------------------------|---------------------------|---------------------------|---------------------------|
| Viscosity (cP) | 324 (18) ^b | 342 (21) ^b | 349 (23) ^{ab} | 379 (24) ^{ab} | 387 (21) ^a |
| Density ($\text{kg}\cdot\text{m}^{-3}$) | 1.221 (0.01) ^a | 1.225 (0.02) ^a | 1.231 (0.02) ^a | 1.237 (0.01) ^a | 1.247 (0.02) ^a |
| pH | 7.6 (0.98) ^a | 7.56 (1) ^a | 7.27 (0.97) ^a | 6.92 (1.1) ^a | 6.5 (0.89) ^a |

Numbers in parentheses are standard deviations (SD). Means, with the same letter, for each evaluated property do not differ (Duncan's test, $p < 0.01$, and an analysis of variance with a 0.01 significance level).

The pH of the nanocomposites was measured by a portable 826-pH mobile (Metrohm, Herisau, Switzerland). The DVE digital-viscometer (Brookfield Ametek, Middleborough, MA, USA) was used to measure the viscosity of the epoxy composite at 20 °C. For this purpose, the spindle was inserted in the container until the epoxy composite level was at the immersion groove on the spindle's shaft. The viscosity was recorded after 120 s with a spindle rotational speed of 10 rpm. The density of the composite was determined based on ASTM D792. The specifications of epoxy resins with different content of M-CNF are reported in Table 1.

2.2.2. Characterization of Functional Groups of M-CNF

The changed functional groups of M-CNF induced by the modification of CNF were investigated by Fourier-transform infrared spectroscopy (FTIR) using an FTIR instrument (Jasco 4700, Tokyo, Japan) from 4000 to 475 cm^{-1} at a resolution of 1 cm^{-1} .

The samples of epoxy nanocomposite with M-CNF were studied using powder X-ray diffraction (XRD) with a copper sealed-tube X-ray source producing Cu α radiation (D8 Advance, Bruker, MA, USA). The samples were measured under radiation at an angular incidence of 4–70° with a scan speed of 3°·min⁻¹. The surface structure of nanocomposites was studied by high-performance field-emission scanning electron microscopy (MIRA3 XMU, TESCAN, Brno, Czech Republic) at a 20 kV accelerating voltage. Before the examination, the samples were coated with 10–20 nm of gold to obtain conductivity.

2.2.3. Mechanical, Physical, and Morphological Assessments

The mechanical properties of the epoxy composites were examined through tensile, flexural, and impact tests utilizing computer-controlled material-testing machines (ZWICK/ROELL, Ulm, Germany). Tensile testing was performed on neat and reinforced epoxy specimens using ASTM D3039 [69]. The sheet-shaped samples, with dimensions of 60 mm × 20 mm × 3 mm in a gauge length of 40 mm, were strained at a rate of 10 mm·min⁻¹. Three-point flexural strength and modulus were measured according to ASTM D790 [70]. Prepared specimens with dimensions of 80 mm × 20 mm × 3 mm located on a span with a length of 60 mm were tested with head speeds of 2 mm·min⁻¹. In addition, the impact strength of a composite was determined using a pendulum-impact testing machine following ASTM D256 [71] with specimens with dimensions of 60 mm × 10 mm × 3 mm placed in a span with a length of 50 mm. The water absorption (WA) and thickness swelling (TS) tests of the composites were performed according to ASTM D570 [72]. Samples with dimensions of 40 mm × 20 mm × 3 mm were completely immersed in a container of distilled water maintained at a temperature of 23 ± 1 °C. For the first 8 h, the amount of water absorption and thickness swelling were measured at two-hour intervals. Then, they were measured once per 24 h for one week. This measurement process continued until there were no more changes from the previous measurement in the weight and thickness of the samples. The final measurement was called the substantially saturated weight and thickness. The substantially saturated weight and thickness minus the dry weight and thickness were considered the WA and TS of the M-CNF/epoxy nanocomposite when substantially saturated. Nine replicate samples were tested at room temperature for each case. The results were studied using analysis of variance, and the means were grouped using Duncan's method.

Scanning electron microscopy (SEM) was used to investigate the surface morphology and distribution of the CNFs in the epoxy matrix. The samples were imaged using a scanning electron microscope Tescan Vega (Tescan Orsay Holding, Brno, Czech Republic) with a 20 kV accelerating voltage after being coated with 10–20 nm of gold.

3. Results

3.1. FTIR Spectroscopy of M-CNF

FTIR spectra were collected to verify the interfacial modification of CNF to obtain M-CNF. As shown in Figure 3a, there was a clear alteration in the spectrum of M-CNF materials. Compared with that of CNF, the relative severity of the peak at 3336 cm⁻¹ significantly decreased in the M-CNF spectrum, indicating that the -OH interfacial functional groups became covered and less effective. Moreover, the absorption bands at 2913 cm⁻¹ belong to asymmetric and symmetric H-C-H stretching vibrations. The 1600–1670 cm⁻¹ bands are related to the stretching vibration of symmetric stretching vibrations of the N-H group [73]. The band at 1427 cm⁻¹ indicates C-C stretching. It can be an indication of growth in the extent of crystalline cellulose. The absorption bands at 1315 and 1368 cm⁻¹ belong to stretching- and bending-mode vibrations of -CH. The bands in the region of 1000–1200 cm⁻¹ are connected to the stretching vibrations of C-O-C and C-O [74–77]. In nanocomposites, the intensity of the oxirane peak (896 cm⁻¹) was reduced with the disappearance of the carbohydrate oxidation peak of CNF (1641 and 1637 cm⁻¹) in M-CNF and CNF-filled epoxy nanocomposites. This suggests that CNF might induce a catalytic curing of oxirane rings of epoxy polymer. The reduced oxirane peak shows the higher level of cross-link density of the epoxy polymer in nanocomposites due to CNF particles, possibly oxidized cellulose in the presence of amine-curing-agent-induced amide bonding. These amidated cellulose molecules may have incorporated covalent bonding with epoxide structure, indicating the presence of the amide group's band at around 1640 cm⁻¹ in nanocomposites. This effect suggests the catalytic effect of CNF in epoxy polymer and may also affect the properties of the composite [78].

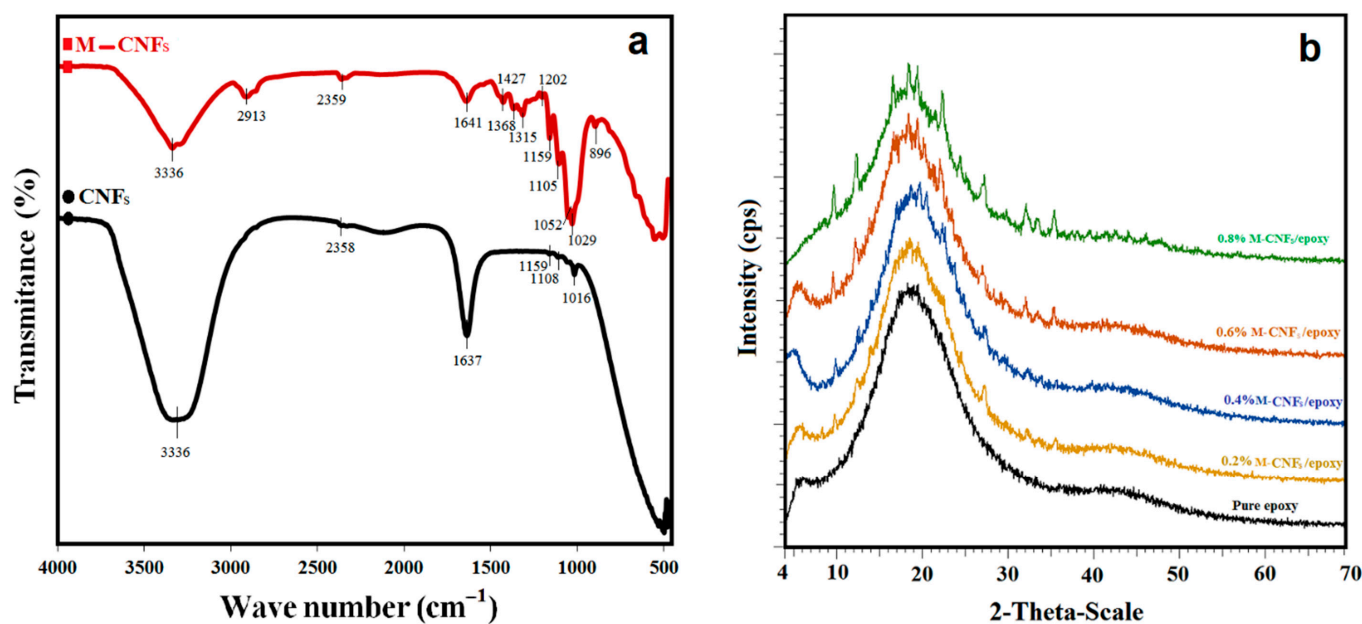


Figure 3. (a) The FTIR spectrum of pure CNF and M-CNF; (b) XRD plots of reinforced epoxy with different concentrations of M-CNF.

3.2. XRD Analysis of Reinforced Nanocomposites

The crystalline structure of epoxy nanocomposites with M-CNF was investigated by XRD analysis; the results are shown in Figure 3b. The characteristic peak of the pure epoxy nanocomposite emerged at a 2θ angle of 20° . XRD patterns showed that despite limited but growing oscillation in the three-dimensional structure of cured reinforced epoxy by the addition of up to 0.8% M-CNFs, there was no alteration to the trans-crystalline phase in the interface region. All CNF/epoxy nanocomposites revealed similar diffraction patterns as the pure epoxy. The characteristic diffraction peak of M-CNF composites demonstrated that the relatively low weight fraction of M-CNF was well surrounded by epoxy. Additionally, the results indicate that the crystalline structure of epoxy resin was not influenced by the introduction of CNF. This indicates that uniform dispersion of M-CNF in the epoxy matrix is mainly attributed to the formation of covalent bonds with the epoxy matrix [79,80].

3.3. Morphological Properties of Epoxy Nanocomposites with M-CNF

The surface morphology of epoxy nanocomposites with M-CNF was studied through scanning electron microscopy (SEM); imaging is displayed in Figure 4. A smooth, glassy, and wavy surface was observed in the micrograph of pure epoxy. The addition of 0.4% M-CNFs to the epoxy matrix makes the surface moderately coarser and rougher than the surface of pure epoxy, but it displays no clumping of fillers. Agglomeration occurred with the addition of 0.8% M-CNF to the epoxy matrix. The agglomeration is caused by extreme cohesive forces between the M-CNF. Despite even scattering of agglomerated clusters of M-CNF in the epoxy matrix, this agglomeration can interrupt the performance of the epoxy nanocomposite and limit the reinforcement impact of M-CNF in epoxy [81]. As previously seen in Figure 2a–e, increasing the M-CNF reduced the transparency of the composite by altering the morphological structure.

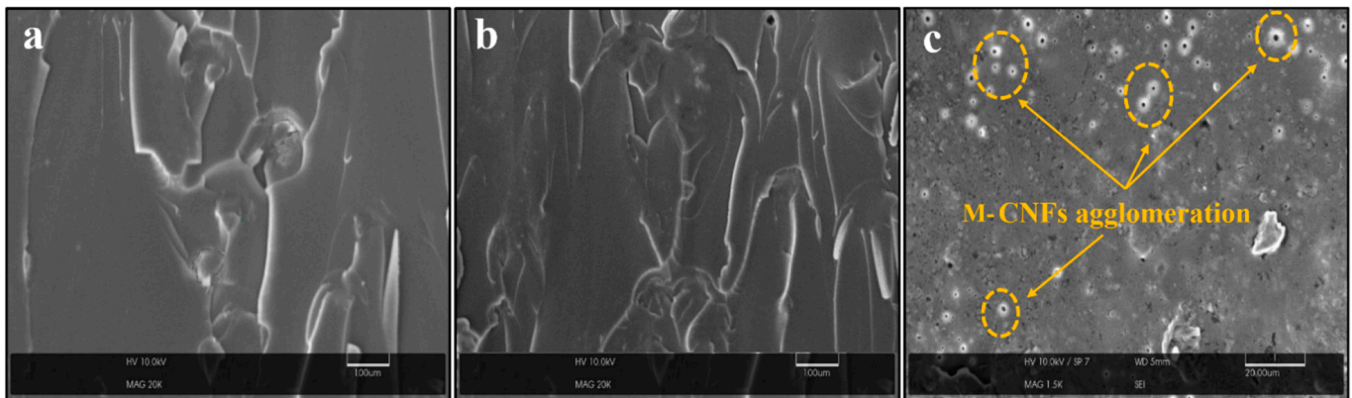


Figure 4. SEM images of (a) pure epoxy resin; (b,c) epoxy resin with M-CNF at (b) 0.4%, (c) 0.8%.

3.4. Performance of Epoxy Nanocomposites with M-CNF

The mechanical and physical characteristics of pure epoxy, as well as its nanocomposites containing 0.2%, 0.4%, 0.6%, and 0.8% M-CNF, are presented in Figure 5. The results showed an improvement in mechanical strength and modulus values for reinforced epoxy nanocomposite samples. In all cases, the performance of the epoxy with M-CNF was significantly ($p < 0.01$) greater than the reference sample. The maximum flexural properties occurred for 0.6% M-CNF content in the epoxy nanocomposite (Figure 5a). There were improvements of 163% and 197% in the flexural modulus and flexural strength, respectively (Figure 5a). Similarly, the tensile modulus and tensile strength increased with M-CNF content up to 0.6%, then decreased at 0.8% (Figure 5b). The best performances for tensile modulus and tensile strength were observed in epoxy nanocomposites with 0.6% M-CNF, where these properties increased by 155%, and 466%, respectively. These results indicated greater improvement for tensile performance compared to flexural performance for the tested nanocomposite containing M-CNF.

Figure 5c shows impact strength with trends relatively analogous to those of the flexural and tensile properties. These improvements in mechanical properties can be attributed to the M-CNF's greater rigidity, stiffness, and well-developed interface region that enhances the epoxy composite's mechanical properties by efficiently transferring the load through the M-CNF interface with epoxy [82]. Regarding the performance of the epoxy nanocomposite with 0.8% M-CNF, some black spots appeared in definite places and this caused the formation of micro-sized cavities within the epoxy matrix. It is noteworthy to mention that sonication at 0.8% M-CNF was not completely effective; so, hydroxyl bonds between nanofibers are stronger than sonication waves preventing the formation of a single fiber–epoxy interaction. This, in turn, leads to a weaker network with dark spots working as crack initiation points (Figure 4c).

In the case of water absorption and thickness swelling, the presence of M-CNF acts as an aggravating factor. Increasing the M-CNF content significantly ($p < 0.01$) elevated the water absorption and resulted in higher TS content. This can be attributed to M-CNF's cavities, porosity, and hydrophilic nature; the micro-porous epoxy nanocomposite trapped the water, leading to an increase in the weight of the epoxy nanocomposite. Furthermore, hydrogen bonds form between water molecules and CNF fillers. This situation was worse for epoxy nanocomposites with 0.8% CNF because of agglomeration, whereas epoxy nanocomposites containing 0.8% M-CNF had WA and TS of 1.49% and 1.57%, respectively, compared to hydrophobic pure epoxy.

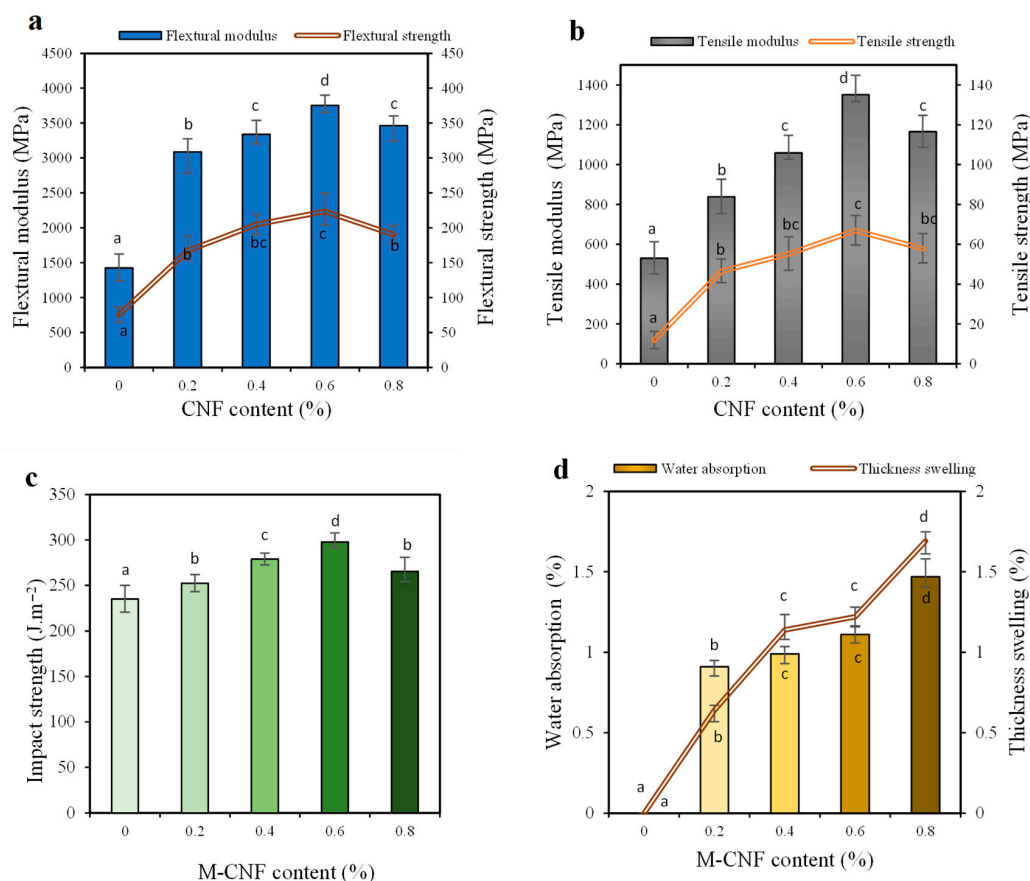


Figure 5. Effect of M-CNF content on the mechanical and physical characteristics of epoxy composites: (a) flexural modulus and flexural strength, (b) tensile modulus and tensile strength, (c) impact strength, and (d) water absorption and thickness swelling (symbols a, b, ab, c and d are indicative of grouping from statistical analysis using Duncan’s method).

4. Conclusions

This paper introduces a novel bio-nano composite made from cellulose nanofiber (CNF)-reinforced epoxy. To enhance the dispersion of CNF in epoxy, we functionalized the CNF surface using a two-step chemical treatment to develop modified cellulose nanofiber (M-CNF). The following conclusions were drawn:

- M-CNF showed enhanced compatibility with the epoxy matrix due to the presence of methyl groups on the surface of M-CNF; these methyl groups enhanced interfacial interactions via hydrogen bonding. This, in turn, led to the uniform dispersion of M-CNF in the epoxy matrix.
- Bio-nano composites containing 6% M-CNF showed enhanced mechanical properties as measured by an increase in strength, modulus, tensile, and impact resistance. The enhancement was most notable for tensile strength, which increased from 11.8 to 66.8 MPa.
- At dosages above 0.6% M-CNF, some weakening effects were observed at the interface due to the self-assembly of cellulose nanofiber; therefore, the optimum dosage is suggested as 0.6%. Self-assembled agglomerates served as crack initiation points as evidenced by crack initiation around agglomerated spots.
- Due to the porosity and hydrophilic nature of cellulose nanofiber, the moisture uptake of the specimen was increased by 100% when 0.6% M-CNF was introduced to the epoxy matrix.

This study provides insights into developing epoxy bio-nano composites that are scalable and cost-effective while taking advantage of cellulose nanofiber. This, in turn,

promotes sustainability and resource conservation in composite manufacturing. In this study, CNFs were modified through solvent exchange of ethanol and acetone in CNFs. A major drawback is the large amount of organic solvents needed. The “greenness” depends on the solvent and is under debate; the huge amount needed is not helpful in this respect and explains the difficulties in industrial implementation.

Author Contributions: M.M.: Conceptualization, Software, Writing—Original Draft, Methodology, Investigation, Formal Analysis. M.F.P.: Writing—Original Draft, Writing—Review and Editing, Methodology, Software, Formal Analysis. H.Y.: Supervision, Methodology. A.D.: Methodology, Writing—Original Draft, Formal Analysis, Writing—Review and Editing. A.J.L.: Writing—Review and Editing. E.F.: Supervision, Writing—Review and Editing. All authors have read and agreed to the published version of the manuscript.

Funding: The author(s) report there is no funding associated with the work featured in this article.

Data Availability Statement: All data and models generated or used during this study appear in the submitted article.

Acknowledgments: The authors are thankful to Gorgan University of Agricultural Sciences and Natural Resources (GUASNR), Gorgan, Iran, and Wood and Forest Products Science Research Division, Research Institute of Forests and Rangelands, Agricultural Research Education and Extension Organization (AREEO), Tehran, Iran for providing research facilities.

Conflicts of Interest: The authors declare no conflicts of interest.

References

- Shanbedi, M.; Ardebili, H.; Karim, A. Polymer-based triboelectric nanogenerators: Materials, characterization, and applications. *Prog. Polym. Sci.* **2023**, *144*, 101723. [[CrossRef](#)]
- Sun, F.; Jiang, H.; Wang, H.; Zhong, Y.; Xu, Y.; Xing, Y.; Yu, M.; Feng, L.-W.; Tang, Z.; Liu, J. Soft fiber electronics based on semiconducting polymer. *Chem. Rev.* **2023**, *123*, 4693–4763. [[CrossRef](#)] [[PubMed](#)]
- Meng, Y.; Xing, S.; Tang, J.; Liu, H.; Lyu, J.; Wang, S.; Yin, C.; Yi, X.; Wu, N. Robust interface-free superhydrophobic polymer-based composites with recoverable and anti-icing properties. *Prog. Org. Coat.* **2023**, *174*, 107224. [[CrossRef](#)]
- Liu, B.; Cao, Q.; Li, J.; Jian, X.; Weng, Z. Facile recycling of anhydride-cured epoxy thermoset under mild conditions with multifunctional hydrazine hydrate. *Chin. Chem. Lett.* **2023**, *34*, 108465. [[CrossRef](#)]
- Verma, C.; Olasunkanmi, L.O.; Akpan, E.D.; Quraishi, M.; Dagdag, O.; El Gouri, M.; Sherif, E.-S.M.; Ebenso, E.E. Epoxy resins as anticorrosive polymeric materials: A review. *React. Funct. Polym.* **2020**, *156*, 104741. [[CrossRef](#)]
- Thajai, N.; Rachtanapun, P.; Thanakkasaranee, S.; Chaiyasao, T.; Phimolsiripol, Y.; Leksawasdi, N.; Sommano, S.R.; Sringarm, K.; Chaiwarit, T.; Ruksiriwanich, W. Antimicrobial thermoplastic starch reactive blend with chlorhexidine gluconate and epoxy resin. *Carbohydr. Polym.* **2023**, *301*, 120328. [[CrossRef](#)] [[PubMed](#)]
- Wang, M.; Ma, L.; Li, B.; Zhang, W.; Zheng, H.; Wu, G.; Huang, Y.; Song, G. One-step generation of silica particles onto graphene oxide sheets for superior mechanical properties of epoxy composite and scale application. *Compos. Commun.* **2020**, *22*, 100514. [[CrossRef](#)]
- Saba, N.; Safwan, A.; Sanyang, M.; Mohammad, F.; Pervaiz, M.; Jawaid, M.; Alothman, O.; Sain, M. Thermal and dynamic mechanical properties of cellulose nanofibers reinforced epoxy composites. *Int. J. Biol. Macromol.* **2017**, *102*, 822–828. [[CrossRef](#)] [[PubMed](#)]
- Abdalla, J.A.; Thomas, B.S.; Hawileh, R.A.; Yang, J.; Jindal, B.B.; Ariyachandra, E. Influence of nano-TiO₂, nano-Fe₂O₃, nanoclay and nano-CaCO₃ on the properties of cement/geopolymer concrete. *Clean. Mater.* **2022**, *4*, 100061. [[CrossRef](#)]
- Chowdhury, M.A.; Hossain, N.; Shuvho, M.B.A.; Kowser, M.A.; Islam, M.A.; Ali, M.R.; Ei-Badry, Y.A.; Ei-Bahy, Z.M. Improvement of interfacial adhesion performance of the kevlar fiber mat by depositing SiC/TiO₂/Al₂O₃/graphene nanoparticles. *Arab. J. Chem.* **2021**, *14*, 103406. [[CrossRef](#)]
- Nobile, M.R.; Valentino, O.; Morcom, M.; Simon, G.P.; Landi, G.; Neitzert, H.C. The effect of the nanotube oxidation on the rheological and electrical properties of CNT/HDPE nanocomposites. *Polym. Eng. Sci.* **2017**, *57*, 665–673. [[CrossRef](#)]
- Huang, F.; Zheng, W.; Rad, A.T.; Nieh, M.-P.; Cornelius, C.J. SiO₂-TiO₂-PBC nanocomposite film morphology, solvent swelling, estimated χ parameter, and liquid transport. *Polymer* **2017**, *123*, 247–257. [[CrossRef](#)]
- He, H.; Li, K.; Wang, J.; Sun, G.; Li, Y.; Wang, J. Study on thermal and mechanical properties of nano-calcium carbonate/epoxy composites. *Mater. Des.* **2011**, *32*, 4521–4527. [[CrossRef](#)]
- Yang, Q.; Lin, Y.-H.; Li, M.; Shen, Y.; Nan, C.-W. Characterization of mesoporous silica nanoparticle composites at low filler content. *J. Compos. Mater.* **2016**, *50*, 715–722. [[CrossRef](#)]
- Velmurugan, R.; Mohan, T. Epoxy-clay nanocomposites and hybrids: Synthesis and characterization. *J. Reinf. Plast. Compos.* **2009**, *28*, 17–37. [[CrossRef](#)]

16. Li, M.; Pu, Y.; Thomas, V.M.; Yoo, C.G.; Ozcan, S.; Deng, Y.; Nelson, K.; Ragauskas, A.J. Recent advancements of plant-based natural fiber–reinforced composites and their applications. *Compos. Part B Eng.* **2020**, *200*, 108254. [[CrossRef](#)]
17. Pandey, J.K.; Lee, H.T.; Takagi, H.; Ahn, S.; Saini, D.; Misra, M. Dispersion of nanocellulose (NC) in polypropylene (PP) and polyethylene (PE) matrix. In *Handbook of Polymer Nanocomposites. Processing, Performance and Application: Volume C: Polymer Nanocomposites of Cellulose Nanoparticles*; Springer: Berlin/Heidelberg, Germany, 2015; pp. 179–189.
18. Thakur, V.K. *Lignocellulosic Polymer Composites: Processing, Characterization, and Properties*; John Wiley & Sons: Hoboken, NJ, USA, 2014.
19. Kargarzadeh, H.; Ahmad, I.; Thomas, S.; Dufresne, A. *Handbook of Nanocellulose and Cellulose Nanocomposites*; John Wiley & Sons: Hoboken, NJ, USA, 2017.
20. Dorieh, A.; Ayrimis, N.; Pour, M.F.; Movahed, S.G.; Kiamahalleh, M.V.; Shahavi, M.H.; Hatefnia, H.; Mehdinia, M. Phenol formaldehyde resin modified by cellulose and lignin nanomaterials: Review and recent progress. *Int. J. Biol. Macromol.* **2022**, *222*, 1888–1907. [[CrossRef](#)] [[PubMed](#)]
21. Dorieh, A.; Khan, A.; Selakjani, P.P.; Pizzi, A.; Hasankhah, A.; Meraj, M.; Pirouzram, O.; Abatari, M.N.; Movahed, S.G. Influence of wood leachate industrial waste as a novel catalyst for the synthesis of UF resins and MDF bonded with them. *Int. J. Adhes. Adhes.* **2021**, *111*, 102985. [[CrossRef](#)]
22. Dorieh, A.; Pour, M.F.; Movahed, S.G.; Pizzi, A.; Selakjani, P.P.; Kiamahalleh, M.V.; Hatefnia, H.; Shahavi, M.H.; Aghaei, R. A review of recent progress in melamine-formaldehyde resin based nanocomposites as coating materials. *Prog. Org. Coat.* **2022**, *165*, 106768. [[CrossRef](#)]
23. Pour, M.F.; Khanjanzadeh, H.; Dorieh, A.; Kiamahalleh, M.V.; Hoseini, K.D. Utilization of phenol formaldehyde/Fe₃O₄ nanocomposite as microwave preheating amplifier in laminated veneer lumber (LVL) structure. *J. Build. Eng.* **2022**, *46*, 103809. [[CrossRef](#)]
24. Islam, M.S.; Pickering, K.L.; Foreman, N.J. Curing kinetics and effects of fibre surface treatment and curing parameters on the interfacial and tensile properties of hemp/epoxy composites. *J. Adhes. Sci. Technol.* **2009**, *23*, 2085–2107. [[CrossRef](#)]
25. Pour, M.F.; Edalat, H.; Dorieh, A.; Kiamahalleh, M.V.; Shahavi, M.H. Durability-related performance of reinforced bondline by phenol formaldehyde/nano SiO₂ composite in Laminated Veneer Lumber (LVL). *J. Build. Eng.* **2022**, *60*, 105191. [[CrossRef](#)]
26. Dorieh, A.; Selakjani, P.P.; Shahavi, M.H.; Pizzi, A.; Movahed, S.G.; Pour, M.F.; Aghaei, R. Recent developments in the performance of micro/nanoparticle-modified urea-formaldehyde resins used as wood-based composite binders: A review. *Int. J. Adhes. Adhes.* **2022**, *114*, 103106. [[CrossRef](#)]
27. Moudood, A.; Rahman, A.; Khanlou, H.M.; Hall, W.; Öchsner, A.; Francucci, G. Environmental effects on the durability and the mechanical performance of flax fiber/bio-epoxy composites. *Compos. Part B Eng.* **2019**, *171*, 284–293. [[CrossRef](#)]
28. Peng, S.X.; Shrestha, S.; Yoo, Y.; Youngblood, J.P. Enhanced dispersion and properties of a two-component epoxy nanocomposite using surface modified cellulose nanocrystals. *Polymer* **2017**, *112*, 359–368. [[CrossRef](#)]
29. Vazquez, A.; Foresti, M.L.; Moran, J.I.; Cyras, V.P. Extraction and production of cellulose nanofibers. In *Handbook of Polymer Nanocomposites. Processing, Performance and Application: Volume C: Polymer Nanocomposites of Cellulose Nanoparticles*; Springer: Berlin/Heidelberg, Germany, 2015; pp. 81–118.
30. Trache, D.; Hussin, M.H.; Chuin, C.T.H.; Sabar, S.; Fazita, M.N.; Taiwo, O.F.; Hassan, T.; Haafiz, M.M. Microcrystalline cellulose: Isolation, characterization and bio-composites application—A review. *Int. J. Biol. Macromol.* **2016**, *93*, 789–804. [[CrossRef](#)] [[PubMed](#)]
31. Negro, C.; Balea-Martín, A.; Sanchez-Salvador, J.L.; Campano, C.; Fuente, E.; Monte, M.C.; Blanco, A. Nanocellulose and its potential use for sustainable industrial applications. *Lat. Am. Appl. Res.-Int. J.* **2020**, *50*, 59–64. [[CrossRef](#)]
32. Camargos, C.H.; Rezende, C.A. Structure–Property relationships of cellulose nanocrystals and nanofibrils: Implications for the design and performance of nanocomposites and all-nanocellulose systems. *ACS Appl. Nano Mater.* **2021**, *4*, 10505–10518. [[CrossRef](#)]
33. Jakob, M.; Mahendran, A.R.; Gindl-Altmutter, W.; Bliem, P.; Konnerth, J.; Mueller, U.; Veigel, S. The strength and stiffness of oriented wood and cellulose-fibre materials: A review. *Prog. Mater. Sci.* **2022**, *125*, 100916. [[CrossRef](#)]
34. Mokhena, T.C.; John, M.J. Cellulose nanomaterials: New generation materials for solving global issues. *Cellulose* **2020**, *27*, 1149–1194. [[CrossRef](#)]
35. Moohan, J.; Stewart, S.A.; Espinosa, E.; Rosal, A.; Rodríguez, A.; Larrañeta, E.; Donnelly, R.F.; Domínguez-Robles, J. Cellulose nanofibers and other biopolymers for biomedical applications. A review. *Appl. Sci.* **2019**, *10*, 65. [[CrossRef](#)]
36. Trache, D.; Tarchoun, A.F.; Derradji, M.; Mehelli, O.; Hussin, M.H.; Bessa, W. Cellulose fibers and nanocrystals: Preparation, characterization and surface modification. In *Functionalized Nanomaterials I*; CRC Press: Boca Raton, FL, USA, 2020; pp. 171–190.
37. Foster, E.J.; Moon, R.J.; Agarwal, U.P.; Bortner, M.J.; Bras, J.; Camarero-Espinosa, S.; Chan, K.J.; Clift, M.J.; Cranston, E.D.; Eichhorn, S.J. Current characterization methods for cellulose nanomaterials. *Chem. Soc. Rev.* **2018**, *47*, 2609–2679. [[CrossRef](#)] [[PubMed](#)]
38. Zhang, S.; Xu, J.; Liu, Z.; Huang, Y.; Jiang, S. Facile, Ecofriendly, and Efficient Preparation of Flexible Gold Nanoparticles@ Bacterial Nanocellulose Surface-Enhanced Raman Scattering Sensors by Magnetron Sputtering for Trace Detection of Hazardous Materials. *ACS Sustain. Chem. Eng.* **2022**, *10*, 13059–13069. [[CrossRef](#)]
39. Milotskiy, R.; Serizawa, R.; Yanagisawa, K.; Sharma, G.; Ito, E.R.D.; Fujie, T.; Wada, N.; Takahashi, K. Composite of Cellulose-Nanofiber-Reinforced Cellulose Acetate Butyrate: Improvement of Mechanical Strength by Cross-Linking of Hydroxyl Groups. *J. Compos. Sci.* **2023**, *7*, 130. [[CrossRef](#)]

40. Zhang, S.; Xu, J.; Liu, Z.; Huang, Y.; Jiang, S. Rapid and scalable preparation of flexible Ag nanoparticle-decorated nanocellulose SERS sensors by magnetron sputtering for trace detection of toxic materials. *Cellulose* **2022**, *29*, 9865–9879. [[CrossRef](#)]
41. Zhang, S.; Xu, J.; Liu, Z.; Huang, Y.; Fu, R.; Jiang, S. Facile and scalable preparation of solution-processed succulent-like silver nanoflowers for 3D flexible nanocellulose-based SERS sensors. *Surf. Interfaces* **2022**, *34*, 102391. [[CrossRef](#)]
42. Thomas, B.; Raj, M.C.; Joy, J.; Moores, A.; Drisko, G.L.; Sanchez, C. Nanocellulose, a versatile green platform: From biosources to materials and their applications. *Chem. Rev.* **2018**, *118*, 11575–11625. [[CrossRef](#)]
43. Sun, X.; Zhu, Y.; Zhu, J.; Le, K.; Servati, P.; Jiang, F. Tough and Ultrastretchable Liquid-Free Ion Conductor Strengthened by Deep Eutectic Solvent Hydrolyzed Cellulose Microfibers. *Adv. Funct. Mater.* **2022**, *32*, 2202533. [[CrossRef](#)]
44. El-Moghazy, A.Y.; Amaly, N.; Istamboulie, G.; Nitin, N.; Sun, G. A signal-on electrochemical aptasensor based on silanized cellulose nanofibers for rapid point-of-use detection of ochratoxin A. *Microchim. Acta* **2020**, *187*, 535. [[CrossRef](#)]
45. Varghese, R.T.; Cherian, R.M.; Chirayil, C.J.; Antony, T.; Kargarzadeh, H.; Thomas, S. Nanocellulose as an Avenue for Drug Delivery Applications: A Mini-Review. *J. Compos. Sci.* **2023**, *7*, 210. [[CrossRef](#)]
46. Kannan, S.; Sahoo, S.K. Influence of flax fiber orientation on mechanical, thermo-mechanical and interfacial adhesion properties of epoxidized methyl ricinoleate modified epoxy composite: A sustainable green composite for cleaner production. *Mater. Today Commun.* **2022**, *33*, 104648.
47. Ojha, A.R.; Biswal, S.K. Thermo physico-mechanical behavior of palm stalk fiber reinforced epoxy composites filled with granite powder. *Compos. Commun.* **2019**, *16*, 158–161. [[CrossRef](#)]
48. Hu, Y.; Zhu, W.; Song, K.; Yu, Z. Fabrication of mechanical robust keratin composites via mussel-inspired surface modification of cellulose nanocrystals. *Mater. Lett.* **2022**, *321*, 132421. [[CrossRef](#)]
49. Moon, R.J.; Martini, A.; Nairn, J.; Simonsen, J.; Youngblood, J. Cellulose nanomaterials review: Structure, properties and nanocomposites. *Chem. Soc. Rev.* **2011**, *40*, 3941–3994. [[CrossRef](#)] [[PubMed](#)]
50. Le Hoang, S.; Vu, C.M.; Pham, L.T.; Choi, H.J. Preparation and physical characteristics of epoxy resin/bacterial cellulose biocomposites. *Polym. Bull.* **2018**, *75*, 2607–2625. [[CrossRef](#)]
51. Neves, R.M.; Ornaghi Jr, H.L.; Zattera, A.J.; Amico, S.C. The influence of silane surface modification on microcrystalline cellulose characteristics. *Carbohydr. Polym.* **2020**, *230*, 115595. [[CrossRef](#)] [[PubMed](#)]
52. Yamato, K.; Yoshida, Y.; Kumamoto, Y.; Isogai, A. Surface modification of TEMPO-oxidized cellulose nanofibers, and properties of their acrylate and epoxy resin composite films. *Cellulose* **2022**, *29*, 2839–2853. [[CrossRef](#)]
53. Trinh, B.M.; Mekonnen, T. Hydrophobic esterification of cellulose nanocrystals for epoxy reinforcement. *Polymer* **2018**, *155*, 64–74. [[CrossRef](#)]
54. Roszowska-Jarosz, M.; Masiewicz, J.; Kostrzewa, M.; Kucharczyk, W.; Żurowski, W.; Kucińska-Lipka, J.; Przybyłek, P. Mechanical properties of bio-composites based on epoxy resin and nanocellulose fibres. *Materials* **2021**, *14*, 3576. [[CrossRef](#)]
55. Sanchez-Salvador, J.L.; Balea-Martín, A.; Negro, C.; Monte, M.C.; Blanco, A. Gel point as measurement of dispersion degree of nano-cellulose suspensions and its application in papermaking. *Nanomaterials* **2022**, *12*, 790. [[CrossRef](#)]
56. Sanchez-Salvador, J.L.; Rasteiro, M.G.; Balea-Martín, A.; Sharma, M.; Pedrosa, J.F.; Negro, C.; Monte, M.C.; Blanco, A.; Ferreira, P.J. Influence of dispersion of fibrillated cellulose on the reinforcement of coated papers. *Int. J. Biol. Macromol.* **2023**, *248*, 125886. [[CrossRef](#)] [[PubMed](#)]
57. Subbotina, E.; Ram, F.; Dvinskikh, S.V.; Berglund, L.A.; Olsén, P. Aqueous synthesis of highly functional, hydrophobic, and chemically recyclable cellulose nanomaterials through oxime ligation. *Nat. Commun.* **2022**, *13*, 6924. [[CrossRef](#)]
58. Frka-Petesic, B.; Parton, T.G.; Honorato-Rios, C.; Narkevicius, A.; Ballu, K.; Shen, Q.; Lu, Z.; Ogawa, Y.; Haataja, J.S.; Droguet, B.E. Structural color from cellulose nanocrystals or chitin nanocrystals: Self-assembly, optics, and applications. *Chem. Rev.* **2023**, *123*, 12595–12756. [[CrossRef](#)] [[PubMed](#)]
59. Song, Q.; Wang, Z.; Xu, D.; Liu, S.; Liu, H.; Zhang, K. Self-assembly of polysaccharide nanocrystals: From aggregation in suspensions to optical materials. *Prog. Polym. Sci.* **2023**, *148*, 101768. [[CrossRef](#)]
60. Zhang, D.; Huang, Y. Dispersion characterizations and adhesion properties of epoxy composites reinforced by carboxymethyl cellulose surface treated carbon nanotubes. *Powder Technol.* **2022**, *404*, 117505. [[CrossRef](#)]
61. Cunha, A.G.; Zhou, Q.; Larsson, P.T.; Berglund, L.A. Topochemical acetylation of cellulose nanopaper structures for biocomposites: Mechanisms for reduced water vapour sorption. *Cellulose* **2014**, *21*, 2773–2787. [[CrossRef](#)]
62. Sehaqui, H.; Zimmermann, T.; Tingaut, P. Hydrophobic cellulose nanopaper through a mild esterification procedure. *Cellulose* **2014**, *21*, 367–382. [[CrossRef](#)]
63. Goussé, C.; Chanzy, H.; Excoffier, G.; Soubeyrand, L.; Fleury, E. Stable suspensions of partially silylated cellulose whiskers dispersed in organic solvents. *Polymer* **2002**, *43*, 2645–2651. [[CrossRef](#)]
64. Zoppe, J.O.; Peresin, M.S.; Habibi, Y.; Venditti, R.A.; Rojas, O.J. Reinforcing poly (ϵ -caprolactone) nanofibers with cellulose nanocrystals. *ACS Appl. Mater. Interfaces* **2009**, *1*, 1996–2004. [[CrossRef](#)] [[PubMed](#)]
65. Boujemaoui, A.; Carlsson, L.; Malmström, E.; Lahcini, M.; Berglund, L.; Sehaqui, H.; Carlmark, A. Facile preparation route for nanostructured composites: Surface-initiated ring-opening polymerization of ϵ -caprolactone from high-surface-area nanopaper. *ACS Appl. Mater. Interfaces* **2012**, *4*, 3191–3198. [[CrossRef](#)]
66. Shimizu, M.; Saito, T.; Isogai, A. Water-resistant and high oxygen-barrier nanocellulose films with interfibrillar cross-linkages formed through multivalent metal ions. *J. Membr. Sci.* **2016**, *500*, 1–7. [[CrossRef](#)]

67. Wang, B.; Torres-Rendon, J.G.; Yu, J.; Zhang, Y.; Walther, A. Aligned bioinspired cellulose nanocrystal-based nanocomposites with synergetic mechanical properties and improved hygromechanical performance. *ACS Appl. Mater. Interfaces* **2015**, *7*, 4595–4607. [[CrossRef](#)] [[PubMed](#)]
68. ASTM D3039; Standard Test Method for Tensile Properties of Polymer Matrix Composite Materials. ASTM International: West Conshohocken, PA, USA, 2002.
69. ASTM D790; Standard Test Methods for Flexural Properties of Unreinforced and Reinforced Plastics and Electrical Insulating Materials. ASTM International: West Conshohocken, PA, USA, 2017.
70. ASTM D256; Standard Test Methods for Determining the Izod Pendulum Impact Resistance of Plastics. ASTM International: West Conshohocken, PA, USA, 2015.
71. ASTM D570; Standard Test Method for Water Absorption of Plastics. ASTM International: West Conshohocken, PA, USA, 1998.
72. Azizi, H.; Eslami-Farsani, R. Study of mechanical properties of basalt fibers/epoxy composites containing silane-modified nanozirconia. *J. Ind. Text.* **2021**, *51*, 649–663. [[CrossRef](#)]
73. Thompson, L.; Nikzad, M.; Sbarski, I.; Yu, A. Esterified cellulose nanocrystals for reinforced epoxy nanocomposites. *Prog. Nat. Sci. Mater. Int.* **2022**, *32*, 328–333. [[CrossRef](#)]
74. Atykyan, N.; Revin, V.; Shutova, V. Raman and FT-IR Spectroscopy investigation the cellulose structural differences from bacteria *Gluconacetobacter sucrofermentans* during the different regimes of cultivation on a molasses media. *AMB Express* **2020**, *10*, 84. [[CrossRef](#)] [[PubMed](#)]
75. Hospodarova, V.; Singovszka, E.; Stevulova, N. Characterization of cellulosic fibers by FTIR spectroscopy for their further implementation to building materials. *Am. J. Anal. Chem.* **2018**, *9*, 303–310. [[CrossRef](#)]
76. Lv, P.; Perre, P.; Perré, G.A. TGA-FTIR analysis of torrefaction of lignocellulosic components (cellulose, xylan, lignin) in isothermal conditions over a wide range of time durations. *BioResources* **2015**, *10*, 4239–4251. [[CrossRef](#)]
77. Pandurangan, M.T.; Kanny, K. Study of curing characteristics of cellulose nanofiber-filled epoxy nanocomposites. *Catalysts* **2020**, *10*, 831. [[CrossRef](#)]
78. Kurita, H.; Ishigami, R.; Wu, C.; Narita, F. Mechanical properties of mechanically-defibrated cellulose nanofiber reinforced epoxy resin matrix composites. *J. Compos. Mater.* **2021**, *55*, 455–464. [[CrossRef](#)]
79. Li, W.; Yao, W.; Wang, J.; Qiu, Z.; Tang, J.; Yang, S.; Zhu, M.; Xu, Z.; Hu, R.; Qin, A. Studying a novel AIE coating and its handling process via fluorescence spectrum. *RSC Adv.* **2017**, *7*, 41127–41135. [[CrossRef](#)]
80. Azhary, T.; Wildan, M.W. Mechanical, morphological, and thermal characteristics of epoxy/glass fiber/cellulose nanofiber hybrid composites. *Polym. Test.* **2022**, *110*, 107560. [[CrossRef](#)]
81. Nissilä, T.; Hietala, M.; Oksman, K. A method for preparing epoxy-cellulose nanofiber composites with an oriented structure. *Compos. Part A Appl. Sci. Manuf.* **2019**, *125*, 105515. [[CrossRef](#)]
82. Yusra, A.I.; Khalil, H.A.; Hossain, M.S.; Davoudpour, Y.; Astimar, A.; Zaidon, A.; Dungani, R.; Omar, A.M. Characterization of plant nanofiber-reinforced epoxy composites. *BioResources* **2015**, *10*, 8268–8280.

Disclaimer/Publisher’s Note: The statements, opinions and data contained in all publications are solely those of the individual author(s) and contributor(s) and not of MDPI and/or the editor(s). MDPI and/or the editor(s) disclaim responsibility for any injury to people or property resulting from any ideas, methods, instructions or products referred to in the content.